JOURNAL OF PROPULSION AND POWER
Vol. 10, No. 5, Sept.–Oct. 1994

On-Orbit Propellant Motion Resulting from an Impulsive Acceleration

John I. Hochstein*
Memphis State University, Memphis, Tennessee 38152
John C. Aydelott†
NASA Lewis Research Center, Cleveland, Ohio 44135
and
Raymond C. Mjolsness‡ and Martin D. Torrey‡
Los Alamos National Laboratory, Los Alamos, New Mexico 87545

In-space docking and separation maneuvers of spacecraft that have large fluid mass fractions may cause undesirable spacecraft motion in response to the impulsive-acceleration-induced fluid motion. An example of this potential low-gravity fluid management problem arose during the development of the shuttle/Centaur vehicle. Experimentally verified numerical modeling techniques were developed to establish the propellant dynamics, and subsequent vehicle motion, associated with the separation of the Centaur vehicle from the shuttle cargo bay. Although the shuttle/Centaur development activity has been suspended, the numerical modeling techniques are available to predict on-orbit liquid motion resulting from impulsive accelerations for other missions and spacecraft.

Introduction

RESEARCH and development to provide the technology base for design and operation of fluid systems in the reduced-gravity environment of space has been actively pursued by NASA for over three decades.[1] This technology program has provided support for the Centaur vehicle development effort in the form of both analytical and experimental studies. During the mid 1980s, the Centaur was modified to make it compatible with the shuttle for launch of the Galileo and Ulysses spacecraft. During this Centaur redesign the dynamics associated with the separation of the Centaur vehicle from the shuttle cargo bay became a concern.

Before separation from the shuttle orbiter, the Centaur vehicle was to be rotated out of the cargo bay by a deployment mechanism attached to the Centaur Integrated Support Structure (CISS). The two vehicles were then to be separated by release of several CISS-mounted springs positioned circumferentially around the aft Centaur structure. These springs would impart a separation force to the Centaur vehicle along its central axis that would yield a differential velocity between the orbiter and the Centaur of approximately 0.3 m/s. However, because of predeployment shuttle maneuvers and atmospheric drag, the propellant in the Centaur vehicle was not likely to be positioned symmetrically with respect to the vehicle axis. Consequently, the resulting spring force at separation probably would not act through the c.g. of the Centaur vehicle, and rotational motion of the Centaur relative to the orbiter could have occurred. A safety concern thus arose over whether this Centaur rotation would be severe enough to cause impact between the Centaur and the CISS or the shuttle orbiter.

This article presents results obtained from an experimental program conducted in the Lewis Zero-Gravity Facility (described in a following section) to study fluid motion resulting from an impulsive acceleration. The data were used to verify numerical modeling techniques that were employed to assess the importance of the Centaur separation dynamics concern. The NASA-VOF3D computer code[2] was employed to perform the numerical modeling. This computer code provides unique treatment of low-gravity, surface-tension-dominated fluid dynamic phenomena so that the propellant motion before and after the application of the accelerating force can be numerically modeled. The computer code predicts not only the propellant motion but also the resulting pressure field in the Centaur propellant tanks. These computer-generated tank pressure fields could be employed in a vehicle dynamics analysis to establish the Centaur motion during separation from the shuttle cargo bay. Because of the relative weights of the liquid hydrogen and oxygen propellants, the influence of the hydrogen propellant motion on the resulting Centaur vehicle motion would have been minimal. Consequently, the experimental and analytical efforts focused on predicting the liquid oxygen propellant motion.

Experimental Program

The major goal of the experimental program was to verify the ability of a numerical model to predict the motion of a liquid and vapor bubble (ullage) when their container is subjected to an impulsive acceleration. An earlier experimental program[3] established possible zero-gravity locations of the oxygen tank vapor bubble prior to Centaur separation. The work reported herein examined the liquid-vapor bubble motion resulting from an impulse similar to, but not scaled to, the separation maneuver. Scaling was not attempted because the shuttle/Centaur program was faced with the challenge of launching the Galileo and Ulysses spacecraft during the second quarter of 1986. Consequently, the program used existing hardware to obtain experimental data in time to support the projected launch date.

Zero-Gravity Facility

The Zero-Gravity Facility consists of a concrete-lined 8.7-m-diam shaft that extends 155 m below ground level (Fig. 1). A steel vacuum chamber, 6.1 m in diam and 142 m high, is contained within the concrete shaft. By using the Lewis wind-tunnel exhaust system in series with vacuum pumps located

Received Aug. 30, 1990; revision received Jan. 26, 1993; accepted for publication Jan. 26, 1993.
*Associate Professor, Mechanical Engineering. Member AIAA.
†Senior Research Engineer, Cryogenic Fluids Technology Office.
‡Staff Member, Fluid Dynamics Group T-3.

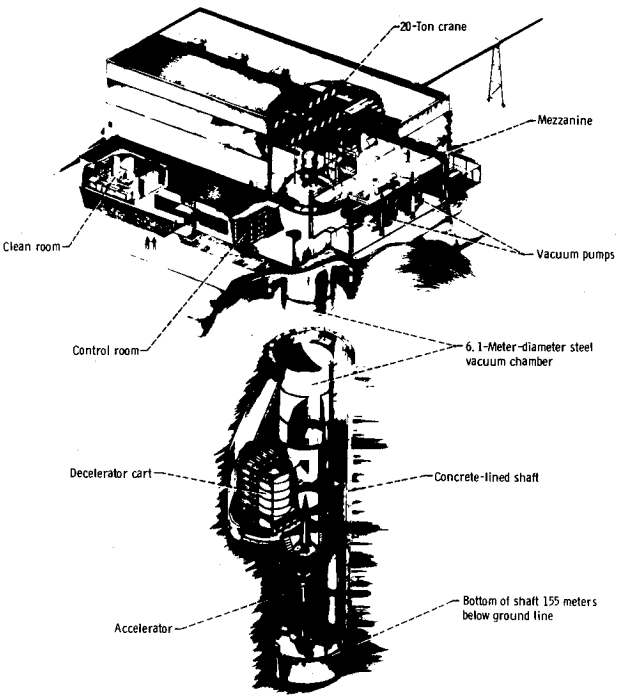

Fig. 1 NASA Lewis Research Center Zero-Gravity Facility.

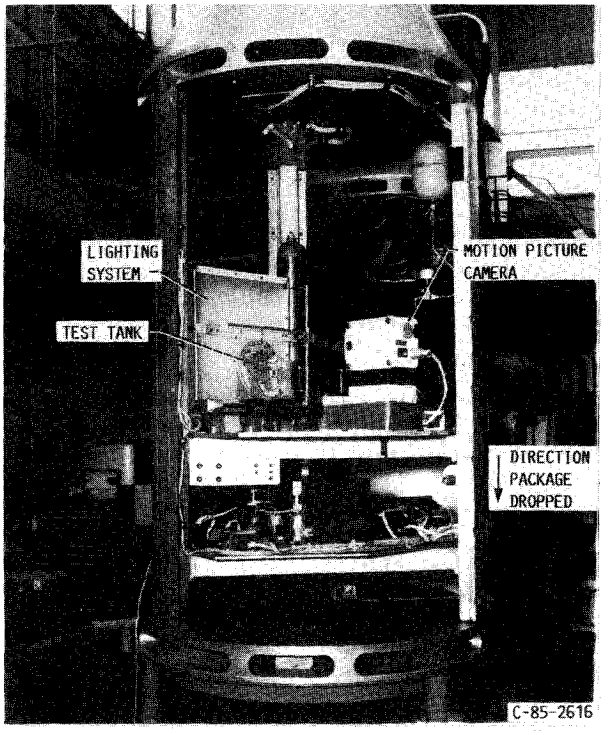

Fig. 2 Zero-Gravity Facility experimental drop package.

in the facility, the pressure in the vacuum chamber is reduced to 13.3 N/m^2 (1.3×10^{-4} atm). Although the residual air in the drop chamber after pumpdown does produce a very low drag on the experimental drop package, this force results in an equivalent acceleration acting on the package that is estimated to be no greater than 10^{-5} g, thus providing an essentially zero-gravity environment. Dropping the package from the top of the chamber provides approximately 5 s of free-fall time. The package is suspended from the top of the vacuum chamber by a support shaft (connected to the cylindrical section of the package) on a hinged-plate assembly. Once chamber pumpdown is completed, the package is released by pneumatically shearing a bolt that holds the hinged plate in a closed position. Following the free-fall period, the package is decelerated at the bottom of the chamber in a cart filled with small pellets of expanded polystyrene. After the drop the vacuum chamber is vented to the atmosphere and the drop package is returned to ground level.

Experimental Drop Package

The experimental drop package (Fig. 2) included a cylindrical section housing the experimental apparatus and the electrical systems. Located below the test tray were 28-V battery packs that supplied and regulated direct current to the experiment.

The hardware mounted on the test tray included a high-speed motion picture camera, digital clock, a lighting system, and the test tank. The test tank was mounted on a cradle fastened to a linear bearing slide assembly. During the drop a lateral force was applied to the test tank by an air cylinder system. The air cylinder consisted of a piston head (inside the cylinder walls) and a piston shaft, which extended beyond the end of the cylinder. The piston shaft was designed to push against the test tank frame, which was held in place with a retaining pin. During the drop the retaining pin was retracted by a solenoid. This allowed the pressurized air cylinder to impart an acceleration to the test tank. The time during which the force was applied to the tank was controlled by adjusting the length of the piston stroke. Once the piston reached the end of its stroke and no longer was in contact with the tank, the tank slid on the linear bearing at a constant velocity.

The length of the linear bearing, and therefore the distance that the tank could travel after being accelerated, was dictated by the experimental drop package dimensions and the need to view the entire carriage displacement. Although it would have been desirable, space was not available on the slide assembly to mount the camera. However, through the use of a wide-angle lens, it was possible to view approximately 27 cm of container motion with the stationary camera. The tank displacement was measured by tracking the motion of pointers attached to the test tank, against a scale with a resolution of 1 mm.

Test Tank and Liquids

The test tank was an oblate spheroid (ellipsoid) formed from a clear acrylic plastic, with semimajor and semiminor axes of 2.00 and 1.47 cm, respectively. This tank geometry was chosen for the test program because of its similarity with the liquid-oxygen tank used on the Centaur vehicle. The experimental conditions and results for all the tests conducted are documented in Ref. 4. Typical results for one of the tests are presented herein. The liquid used in this zero-gravity test, ethanol, exhibited a near 0-deg contact angle on the spheroidal tank walls, as does liquid oxygen on the Centaur tank surface. Other key properties of the liquid (surface tension, density, and viscosity) are presented in Table 1.

Test Setup and Procedure

Before each series of tests the test tank was cleaned ultrasonically to avoid surface contamination. Immediately before each test the tank was rinsed with a solution of distilled water, dried in a warm air dryer, and then rinsed with the test liquid.

Table 1 Liquid properties

Liquid	Surface tension, dyne/cm	Density, g/cm^3	Dynamic viscosity, cP
Ethanol at 20°C	22.3	0.79	1.20
Liquid oxygen at −180°C	10.0	1.07	0.19

Table 2 Summary of zero-gravity facility experimental conditions and anticipated shuttle/Centaur deployment conditions for Galileo mission

Test	Liquid	Fill level, %	Induced acceleration, g	Duration of acceleration, s
1	Ethanol	90	0.25	0.101
Shuttle/Centaur	LO_2	80	0.133[a]	0.440

[a]Maximum value (applied acceleration = 0.133 cos 3.47t, where t denotes time in s).

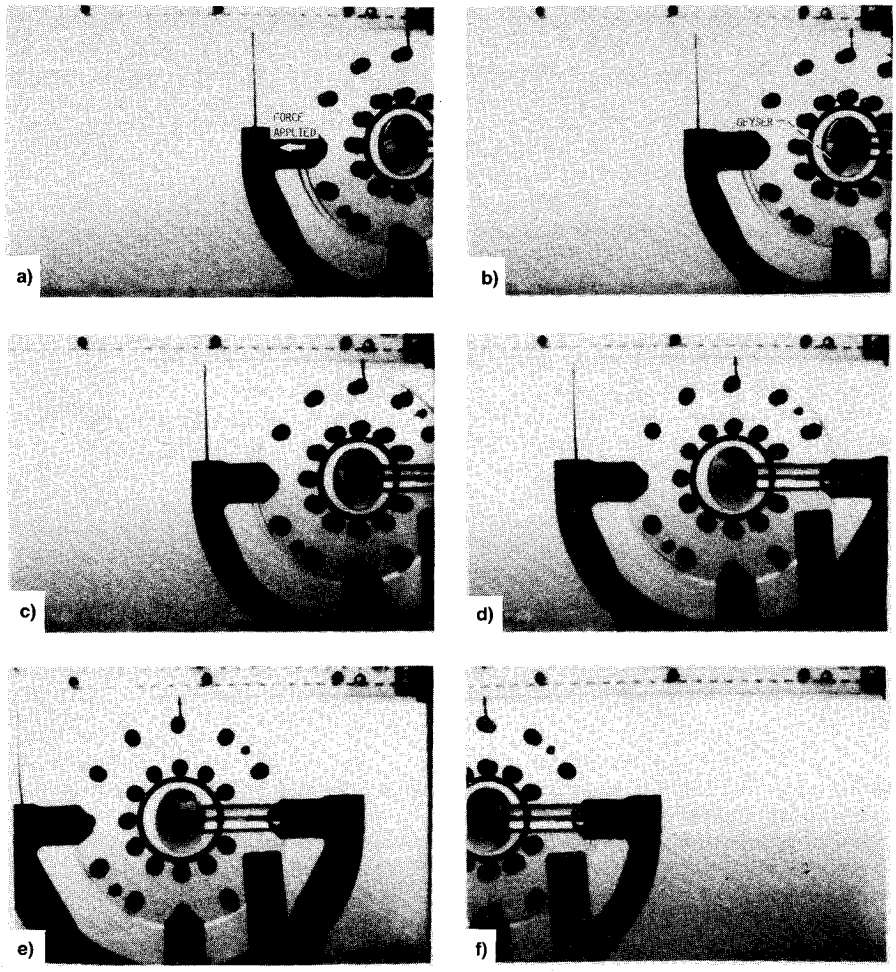

Fig. 3 Liquid-vapor interface configuration during and after impulsive acceleration. Test 1; fill level, 90%; impulse, 0.25 g for 0.101 s (time measured from start of impulsive acceleration): a) initial motion of interface, time, 0.06 s; b) geyser formation; time, 0.10 s; c) maximum interface distortion, time, 0.18 s; d) transient interface shape after acceleration ends, time, 0.40 s; e) movement of interface along tank major axis during constant-velocity period of tank motion, time, 0.62 s; and f) interface again dominated by capillary forces, time, 1.09 s.

After rinsing, the tank was filled to the desired liquid level with a syringe, hermetically sealed, and mounted in the test vehicle.

The entire test vehicle was balanced and the cradle on which the test tank was mounted was leveled to ensure that the ellipsoidal tank was oriented properly before and during the drop. After the tank was mounted and the vehicle balanced, the entire drop package was suspended from the top of the facility. The facility vacuum chamber was then closed and pumped down and the drop package was released. At package release the lights and the motion picture camera were activated. Approximately 2 s after release, a lateral acceleration was applied to the experimental apparatus, and the test tank traversed the linear bearing.

Data Analysis

The data obtained in this investigation were collected during the free-fall period by a high-speed motion picture camera. Information on the zero-gravity liquid-vapor interface configuration was taken from the film by using a film analyzer. From the analyzer the observed interface shape could be directly plotted at various times throughout the drop. In the test films the general outline of the interface was defined by a dark band. The points used for plotting the interface shape followed the outer perimeter of this dark band. The experimental conditions for test 1 and for the anticipated shuttle/Centaur deployment are presented in Table 2.

Owing to the effects of both refraction and parallax, considerable expertise is required to accurately determine the position of the tank and of the liquid/vapor interface as a function of time. The experimental and analytical techniques required to achieve this are discussed in detail, and some data displaying satisfactory results are presented.[4]

In order to understand the problems associated with the dynamics of low-gravity liquid-vapor systems in ellipsoidal tanks, the initial liquid-vapor interface location prior to an

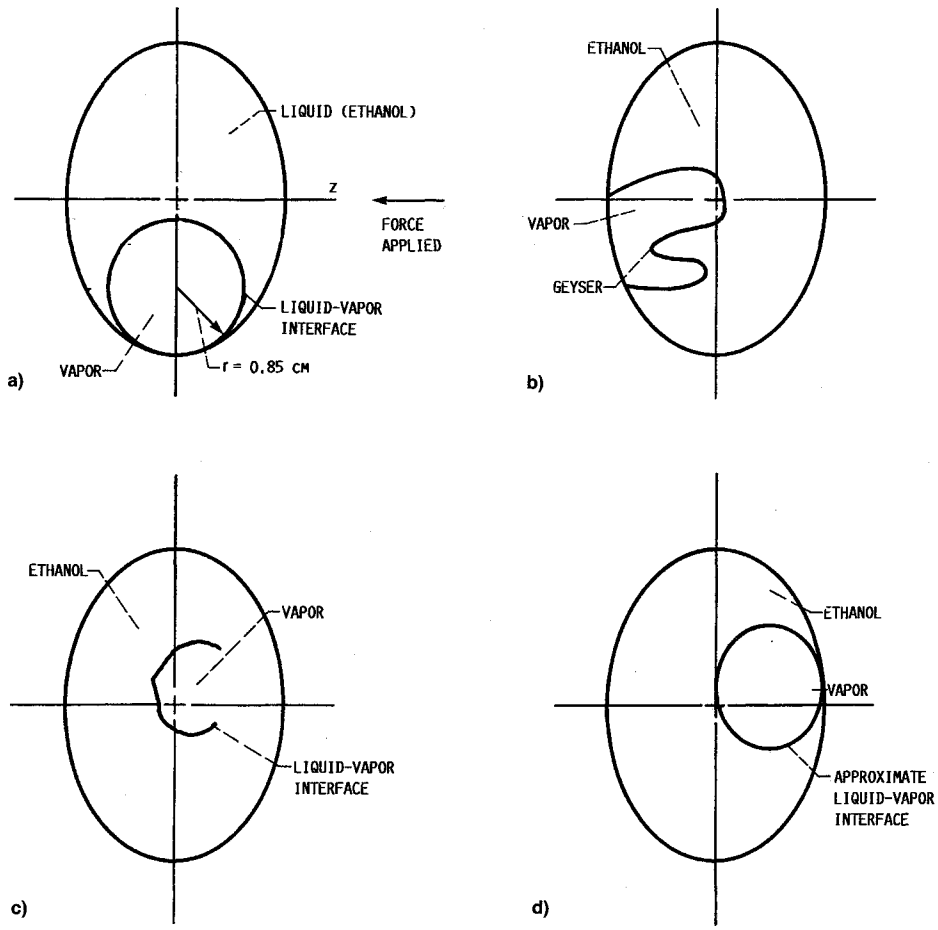

Fig. 4 Plots of liquid-vapor interface configuration—Test 1. Fill level, 90%; impulse, 0.25 *g* for 0.101 s (time measured from start of impulsive acceleration): a) equilibrium zero-gravity configuration. Qualitative view of liquid-vapor interface, time, b) 0.10, c) 0.62, and d) 1.09 s.

imposed disturbance must be known. The initial phase of the test program[3] was performed with the objective of determining equilibrium zero-gravity interface configurations that could exist in an ellipsoid. During the first phase of the study the test tank was not given an acceleration, but instead was clamped to the linear bearing in a fixed position such that the tank was aligned with the optical axis of the motion picture camera. The zero-gravity environment, (drag on the experimental package has an insignificant effect on the results), coupled with solid-liquid-vapor combinations that produced near 0-deg static contact angles, resulted in spherical liquid-vapor interface shapes inside the ellipsoidal tank.

The results presented in Ref. 3 indicate that, depending on the size of the vapor bubble, the liquid-vapor interface can exist at several locations in an ellipsoidal tank. This is true as long as the interface is able to meet the minimum energy requirement by forming a sphere within the walls of the tank. For the shuttle/Centaur separation dynamics problem, only liquid fill levels greater than 70% were of interest. Liquid fill levels of 80% or more resulted in vapor bubbles with diameters small enough to be accommodated anywhere within the tank boundaries. As the interface radius of curvature increased with reduced fill levels, between 80–70%, the vapor bubble tended to form in the center of the ellipsoidal tank since this was the only location where a spherical bubble could fit within the tank boundaries.

After a better understanding of the equilibrium zero-gravity interface configurations had been acquired,[3] the experimental investigation continued by applying a lateral acceleration to the ellipsoidal tank. For the test results presented herein, the orientation of the tank relative to the gravitational vector was selected so that the resulting zero-gravity vapor bubble would be at the assumed worst-case location (that is, at the farthest extreme from the center of the tank, thus providing a maximum c.g. offset) before the start of the impulsive acceleration. During each test sequence the start of the lateral acceleration was delayed by 2.0–2.5 s to allow the liquid-vapor interface to form its zero-gravity configuration. This formation period was sufficiently short to allow adequate time to view the lateral acceleration of the test tank and the resulting motion of the tank and the test fluid.

A number of tests are discussed in detail in Ref. 4. Here, we restrict attention to the later stages of test 1, just before, during, and after the application of the lateral acceleration. Just after the acceleration was initiated, the vapor bubble started to move from the bottom of the tank toward the left wall (Fig. 3a). (The force was applied to the right side of the tank as viewed from the camera.) After the force had acted for approximately 0.1 s, a geyser appeared to form and the vapor bubble became highly deformed (Fig. 3b). When the piston reached the end of its stroke and the applied force was no longer present, the geyser collapsed—leaving a liquid/vapor interface that appeared to have no distinct shape (Fig. 3c). However, in a very short time (approximately 0.4 s) after the acceleration became zero, the interface again appeared to be dominated by capillary forces and started to take on a spherical shape (Fig. 3d). As the ellipsoidal tank continued to move across the track, the interface traveled from the left to the right side of the tank (Fig. 3e). The tank velocity should be approximately constant during this coast period: a low friction linear bearing was used to support the tank, and the tank speed is so low that aerodynamic drag is negligible compared to the inertia of the tank. Toward the end of the drop period the liquid motion damped, and the liquid-vapor in-

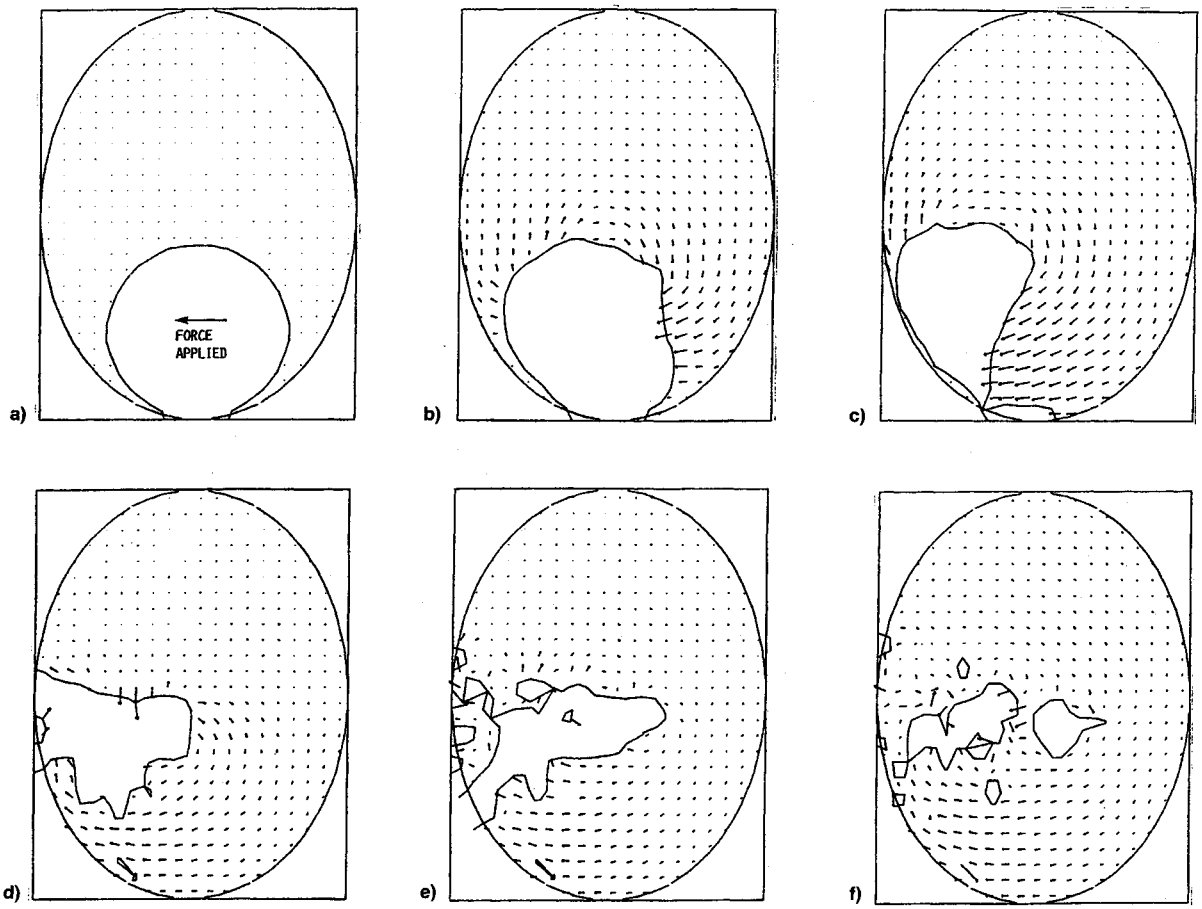

Fig. 5 Numerical modeling of liquid and vapor motion in response to impulsive acceleration—Test 1. Fill level, 90%; impulse, 0.25 *g* for 0.101 s: a) liquid-vapor interface configuration before start of impulsive acceleration. Interface configuration and liquid velocity vectors, b) 0.05, c) 0.10, d) 0.25, e) 0.35, and after impulse initiation f) 0.60 s after impulse initiation; maximum velocity ≈ 15, 27, 10, 7, and 5 cm/s, respectively.

terface appeared to be again forming an equilibrium spherical zero-gravity configuration (Fig. 3f).

Figure 4 presents plots of the liquid-vapor interface corresponding to some of the photographs just described. Figure 4a illustrates the initial condition of the low-gravity liquid/vapor interface before the impulse was applied. This plot was derived from the first phase of the experimental program.[3] Figures 4b and 4d correspond to times when the interface was distorted by refraction and parallax, and therefore are qualitative interpretations of the observed interface. A more accurate interface shape was plotted when the tank was near the middle of the track (Fig. 4c). Note that this plot is not complete, however, because refraction was particularly high near the edge of the ellipsoidal tank.

This part of the program was performed to provide data for the verification of a computer code and did not actually scale the Centaur tank configuration or flight conditions. Time constraints permitted performance of only a limited number of tests. Consequently, no attempt was made to develop correlating parameters relating the influence of the impulsive lateral acceleration to the observed behavior of the liquid and the vapor within the test tank.

Numerical Modeling

The NASA-VOF3D computer code[2] was used to provide 1) an analytical comparison with the results from the previously described tests; and 2) an analytical prediction of the Centaur liquid oxygen motion resulting from the deployment of the vehicle from the shuttle cargo bay, assuming a worst-case initial location for the vapor bubble. The NASA-VOF3D program models three-dimensional incompressible flows with free surfaces by using the volume-of-fluid (VOF) algorithm. It is specifically designed to predict liquid flows in a low-gravity environment, where the free surface physics must be accurately treated. The computational technique is based on the use of donor-acceptor differencing to track the free surface across a Eulerian grid.

The structure of NASA-VOF3D,[2] its relations to predecessor codes,[5,6] and its algorithms for solving the Navier-Stokes equations, convecting the scalar F describing the volume-of-fluid in each computational cell, and the determination of the fluid-vapor interface geometry are all described in Ref. 4. The discussion presented there is sufficiently extensive to provide a useful introduction to the numerical modeling techniques employed, but is still much briefer than the presentations given in Refs. 2, 5, and 6.

Numerical Methodology

This section describes the unique numerical methods for modeling the surface physics, i.e., the surface tension and the wall adhesion, in the NASA-VOF2D and VOF3D computer codes. All the surface physics algorithms developed for NASA-VOF2D were improved and generalized during the development of the three-dimensional modeling capability. In two dimensions one surface curvature can be calculated algebraically, and one curvature must be computed by finite difference approximations. Moreover, the algebraically determined curvature is typically the larger one in the crucial near-axis cells. In three dimensions, both surface curvatures must be computed by less accurate finite-difference approximations. In addition, considerable refinement of the two-dimensional surface tension algorithms was necessary during the development of the three-dimensional computer code. Reference

2 contains a detailed discussion of how these surface physics effects were accounted for numerically.

Although realistic wall adhesion algorithms (a standard feature of NASA-VOF2D) are essential to calculate flow features such as the leading-edge liquid velocity in a propellant reorientation problem, the current version of the three-dimensional program does not permit the accurate calculation of wall adhesion except when the solid boundary coincides with a cell boundary. The inclusion of a realistic wall adhesion calculation into the surface physics routines is one of the principal tasks that must be accomplished if NASA-VOF3D is to evolve into a truly general-purpose code. However, it is emphasized that the present programs still have a significant range of applicability that permits a wide range of design questions to be meaningfully addressed.

Analytical Results and Discussion

The Zero-Gravity Facility Test 1 was numerically modeled. Inputs to the NASA-VOF3D computer code included liquid properties (Table 1), tank geometry, vapor bubble size and location before the start of the impulsive acceleration, and duration, direction, and magnitude of the applied acceleration.

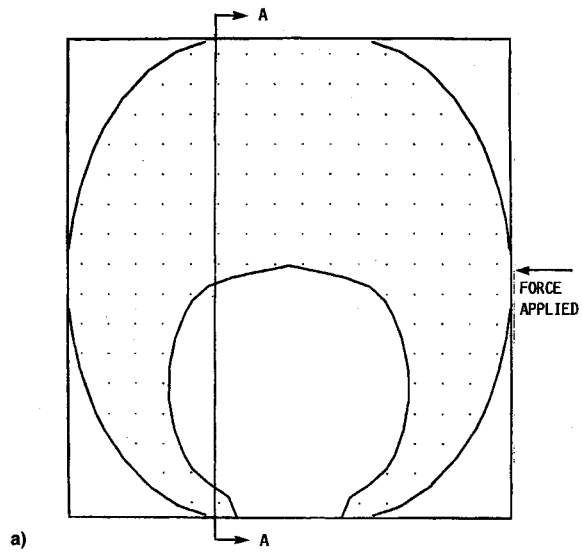

Fig. 6 Numerical modeling of Centaur liquid-oxygen propellant motion during separation maneuver. Initial assumed worst-case liquid-vapor interface configuration; fill level, 89%, impulse applied for 0.44 s with maximum acceleration of 0.133 *g*: a) cross-sectional view of liquid-oxygen tank and b) section A-A.

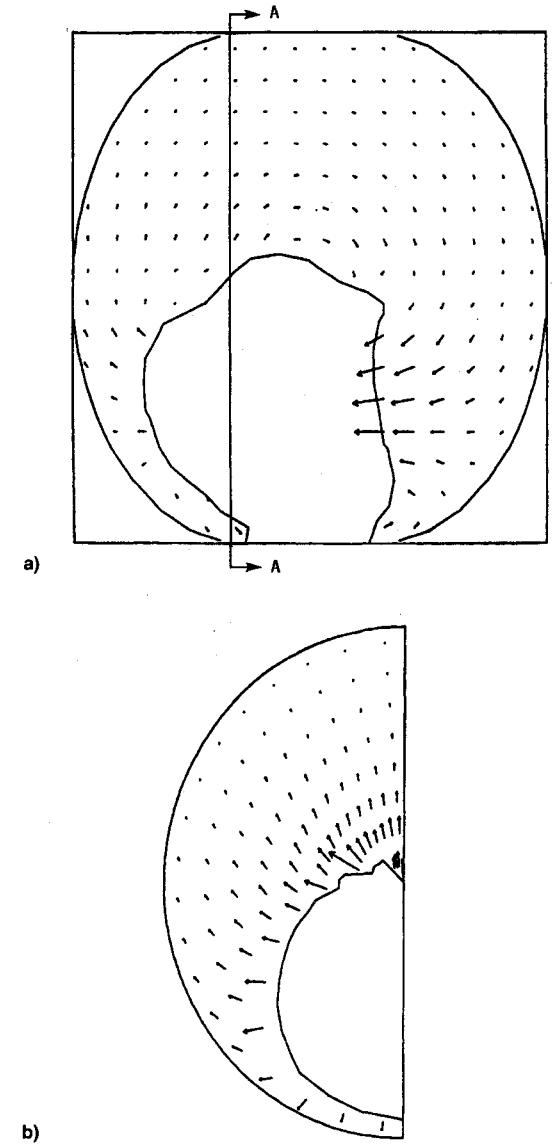

Fig. 7 Numerical modeling of Centaur liquid-oxygen propellant motion during separation maneuver. Time, 1.0 s after impulse initiation; maximum velocity ≈ 50 cm/s: a) cross-sectional view of liquid-oxygen tank and b) section A-A.

The computational results are shown in Fig. 5 as cross-sectional views through the center of the tank. The two-dimensional views of the vapor bubble and the liquid velocity vectors shown are a graphical output feature of the NASA-VOF3D computer code. The liquid velocity vectors are scaled to the maximum liquid velocity for each time step. The sequence in time of the first, third, and last cross-sectional views of the vapor bubble shown in Fig. 5 was selected to correspond approximately in time with the plots of the experimental data presented in Figs. 4a–4c. The numerical modeling was terminated at approximately 0.6 s (Fig. 5f) when significant vapor bubble motion was no longer observed and the vapor bubble began to break up. Comparing the experimental data generated in the Lewis Zero-Gravity Facility with the NASA-VOF3D numerical modeling output led to the conclusion that the computer code could be used to predict liquid-oxygen motion in the Centaur vehicle. Excellent agreement exists between the experimental and numerical results for the duration of the accelerating force. During this time most of the liquid motion took place and the highest liquid velocities were calculated. At later times, in contrast to the experimental observations, the numerically generated ullage fragmented, probably reflecting the continuing difficulty in accurately

modeling surface-tension-dominated fluid dynamic phenomena. However, before the ullage broke up, the liquid motion had significantly subsided, as observed experimentally and predicted numerically. Since the liquid momentum flux is proportional to the square of the liquid velocity, this numerical inaccuracy (ullage fragmentation) should not affect the ultimate objective, the prediction of the liquid-oxygen propellant and Centaur vehicle motion in response to an impulsive acceleration.

Similar to the numerical modeling of the experimental data from the Zero-Gravity Facility, the NASA-VOF3D computer code was employed to predict the liquid-oxygen motion in the Centaur vehicle[7] during a deployment maneuver. Inputs to the code included liquid-oxygen properties (Table 1), the vapor bubble geometry and initial (assumed worst-case) location, the tank geometry, and the characteristics of the separation acceleration (Table 2).

The results of the NASA-VOF3D modeling effort for the shuttle/Centaur program are shown in Fig. 6. The left portion of the figure is a side view of the liquid-oxygen tank showing a cross section through the Centaur vehicle centerline. (Note

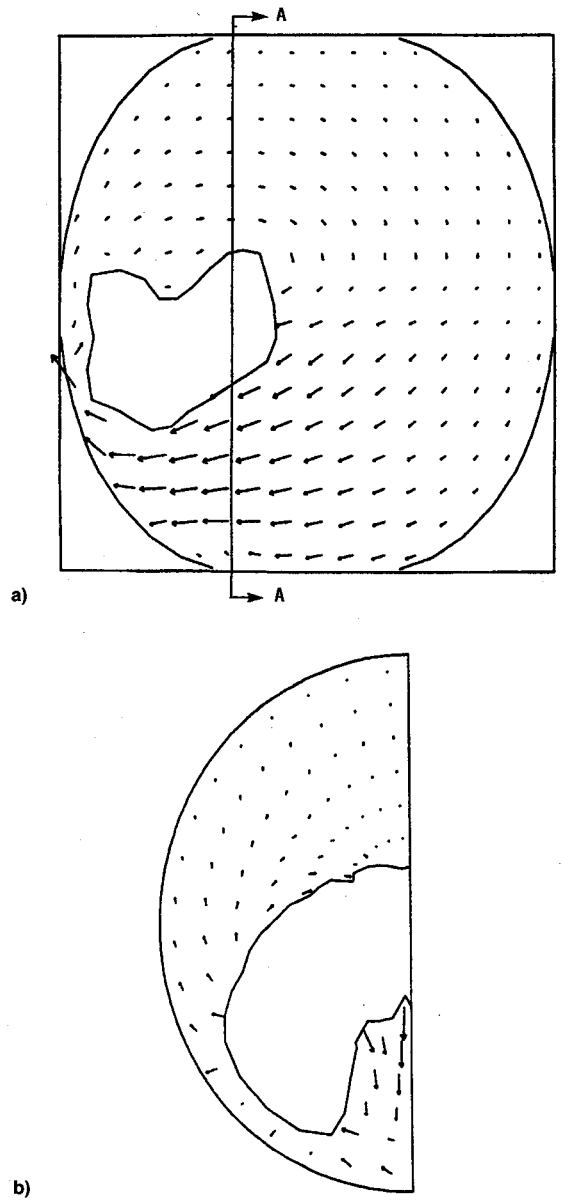

Fig. 8 Numerical modeling of Centaur liquid-oxygen propellant motion during separation maneuver. Time, 10 s after impulse initiation: maximum velocity ≈ 12 cm/s: a) cross-sectional view of liquid-oxygen tank and b) section A-A.

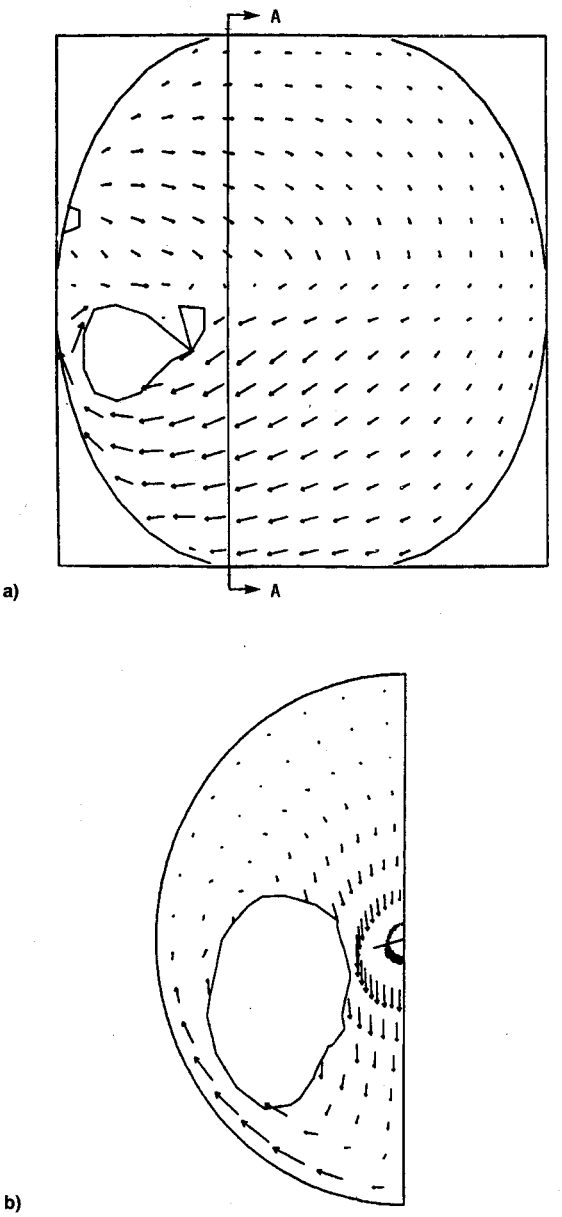

Fig. 9 Numerical modeling of Centaur liquid-oxygen propellant motion during separation maneuver. Time, 20 s after impulse initiation; maximum velocity ≈ 12 cm/s: a) cross-sectional view of liquid-oxygen tank and b) section A-A.

that, in contrast with the oblate spheroid tank configuration used for the experimental tests, the shuttle/Centaur liquid-oxygen tank has been enlarged by the addition of a cylindrical midsection so that it appears to be nearly spherical.) The right side of the figure is a cross-sectional view of the tank that is perpendicular to the Centaur vehicle centerline and taken in a plane approximately one-third of the tank height from the top of the tank. Figure 6 shows the assumed worst-case initial location for the vapor bubble. One second after the start of the 0.44-s duration impulsive acceleration, the liquid velocity reached a maximum of approximately 50 cm/s (Fig. 7). As time progressed (Figs. 8–10), the liquid velocities decayed and the vapor bubble became highly distorted, nearly separating into two distinct regions.

The numerical output of the NASA-VOF3D computer code included the prediction of the pressure distribution in the Centaur liquid-oxygen tank as well as the liquid velocity fields shown graphically in Figs. 7–10. These pressure distribution predictions can be employed in a vehicle dynamics analysis to establish the relative motion of the Centaur and shuttle

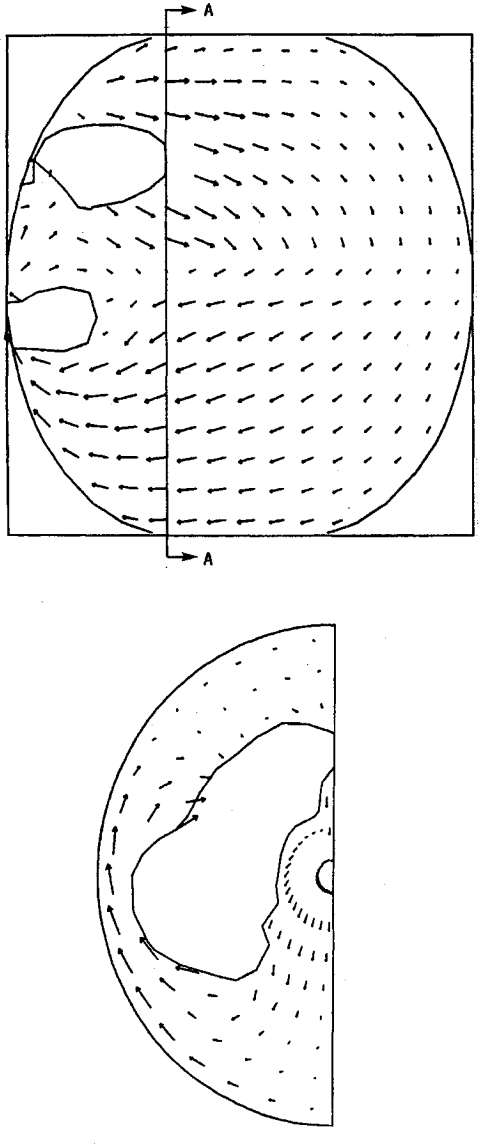

Fig. 10 Numerical modeling of Centaur liquid-oxygen propellant motion during separation maneuver. Time, 40 s after impulse initiation; maximum velocity ≈ 7 cm/s: a) cross-sectional view of liquid-oxygen tank and b) section A-A.

vehicles during a deployment maneuver. For the first two planned Centaur in-shuttle missions—the launches of the Galileo and Ulysses spacecraft—no hazardous vehicle motion was predicted.

Concluding Remarks

Analytical and experimental efforts have addressed the potential problem associated with the separation of the Centaur vehicle from the shuttle orbiter. Experimental data obtained in the Lewis Zero-Gravity Facility were used to assess the capabilities of the NASA-VOF3D computer code. The NASA-VOF3D program was then employed to predict the liquid-oxygen propellant motion and pressure field within the Centaur tankage during the planned deployment maneuver.

Based on the experimental and analytical work performed, it was concluded that no hazardous vehicle motion would have resulted from the Centaur separation maneuver if the propellant tanks were nearly full. Although the shuttle/Centaur development activity has been suspended, the problem solution presented serves to document experimentally observed ullage motion in a reduced gravity environment and the ability of the NASA-VOF3D code to computationally model such flows.

References

[1]Aydelott, J. C., Carney, M. J., and Hochstein, J. I., "NASA Lewis Research Center Low-Gravity Fluid Management Technology Program," NASA TM-87145, 1985; also AIAA/GNOS-85-002, Nov. 1985.

[2]Torrey, M. D., Mjolsness, R. C., and Stein, L. R., "NASA-VOF3D: A Computer Program for Three-Dimensional Incompressible Flows with Free Surfaces," Los Alamos National Lab., Rept. LA-11009-MS, Los Alamos, NM, 1987.

[3]Carney, M. J., "Liquid-Vapor Interface Locations in a Spheroidal Container Under Low-Gravity," NASA TM-87147, 1986.

[4]Aydelott, J. C., Mjolsness, R. C., Torrey, M. D., and Hochstein, J. I., "Numerical Modeling of On-Orbit Propellant Motion Resulting from an Impulsive Acceleration," NASA TM-89873, Jan. 1987; also AIAA Paper 87-1766, Jan. 1987.

[5]Hotchkiss, R. S., "Simulation of Tank Draining Phenomena with the NASA SOLA-VOF Code," Los Alamos National Lab., Rept. LA-8163-MS, Los Alamos, NM, 1979.

[6]Torrey, M. D., Cloutman, L. D., Mjolsness, R. C., and Hirt, C. W., "NASA-VOF2D: A Computer Program for Incompressible Flows with Free Surfaces," Los Alamos National Lab., Rept. LA-10612-MS, Los Alamos, NM, 1985.

[7]*Shuttle/Centaur G-Prime Phase III Safety Review Package Book 2, Airborne Technical Description*, General Dynamics Space Systems Div., Rept. GDSS-SSC85-007, San Diego, CA, 1985.